Specimen representation on the prediction of artificial test lightning plasma, resulting specimen loading and subsequent composite material damage

Specimen Representation on the Prediction of Artificial Test Lightning Plasma, Resulting Specimen Loading and Subsequent Composite Material Damage

S.L.J. Millen[a], A. Murphy[a+], G. Abdelal[a], G. Catalanotti[a]

[a] School of Mechanical and Aerospace Engineering, Queen's University Belfast, Ashby Building, Belfast. Northern Ireland, U.K. BT9 5AH

[+] Corresponding author: Tel.: +44 28 9097 4095; E-mail: a.murphy@qub.ac.uk

Abstract

Preceding work has established that artificial test lightning plasma and composite test specimen damage can be modelled. However, no work has studied the impact of specimen representation in the modelling of the plasma and the resulting impact on specimen damage. Herein four distinct specimen designs have been modelled to understand the impact on plasma properties. The resulting specimen surface loads have then been passed to Finite Element (FE) damage models to predict thermal damage. A magnetohydrodynamic FE multiphysics model is employed to simulate the plasma and a FE thermal-electric modelling approach is used to predict the composite material damage. For the test arrangements modelled herein it has been found that specimen representation has limited impact on plasma global structure, even with significant change in specimen properties (e.g. from copper to epoxy). However, noteworthy variation in the local specimen surface loading is witnessed with specimen property change (e.g. epoxy to carbon reinforced epoxy), with peak magnitudes for surface pressure, velocity, current density and temperature changing by up to 88%. Such variation in local surface loading does significantly vary the prediction of thermal damage depth (up to 1200%) and surface damage area (up to 1314%). This work, for the first time, provides predictions for the thermal damage suffered by both protected and unprotected specimens exposed to test standard Waveform B.

Keywords

Lightning Strike; Magnetohydrodynamics; Aerospace Materials; Thermal Plasma; Finite Element Modelling; Composite Damage;

1.0 Introduction

Lightning strikes are a natural phenomenon that can have a detrimental impact on the composite structure of an aircraft. Lightning occurs during extreme weather events and forms a plasma channel. Ionization is the process that forms plasma, the fourth state of matter, and is caused by radiation or heating such as that within a lightning current channel. Temperatures inside this channel can exceed 10,000^{o}C, with the channel containing many particles including electrons, ions and photons at different states of excitation [1]. Electrical conduction is high in plasma due to the availability of free electrons. In real world lightning events the plasma can last between microseconds and seconds with equivalent variation in the current magnitude and current waveform.

In order to design aircraft to withstand lightning strikes, test standards have been defined with four artificial test lightning Waveforms (A, B, C and D), proposed in SAE-ARP5412B [2] and illustrated in Figure 1. Waveform A is characterised as the first return stroke; Waveform B is the intermediate current; Waveform C is the long duration current; and Waveform D is a subsequent stroke [2]. These Waveforms have distinct time periods and amplitudes presenting their own unique testing and modelling challenges.

Simulations have progressed to model the behaviour of the plasma formed during an artificial lightning test [3]–[5]. Plasma simulations are typically based on Magnetohydrodynamics (MHD). MHD is the analysis of the mutual interaction between fluid flow and magnetic fields. MHD combines three distinct sets of partial differential equations; Maxwell's equations of electromagnetism, Navier-Stokes equations of fluid motion, and thermal conduction equations for heat transfer. These partial differential equations can be solved numerically using the Finite Element (FE) method or the finite volume method. Moreover many works have presented FE modelling methods for the prediction of damage within composite specimens resulting from assumed artificial test lightning current, temperature and pressure loading. However, few works have combined the modelling of plasma and the mechanics of specimen material damage. Thus limited understanding exists on the influence of plasma modelling on the

prediction of specimen damage, and vice versa. This paper aims to understand the impact of specimen representation on the formation of artificial test lightning plasma and relate this to specimen loading and subsequent specimen composite material damage.

2.0 Background

2.1 Lightning strike experimental research

Lightning strike experimental research has typically used the standardised waveforms from SAE-ARP5412B [2] which define the impulse waveform including the maximum current (I_{max}), the rise time from 10% to 90% of the maximum current (T1) and the time to reach the post-peak value of 50% of the maximum current (T2). Preceding experimental works have used a conical tip discharge probe, the cathode, positioned a few millimetres above the centre of the specimen and a copper plate below the specimen, the anode, to generate the lightning plasma [6]–[8]. Feraboli et al. [6], [9] investigated the influence of strikes on specimens with and without fasteners while Wang et al. [10] compared the damage area for three test cases with different aluminium protection systems. However, the majority of authors have focussed on unprotected specimens with varying current loads and time periods derived from Waveform A [7], [8], [11], [12].

2.2 Lightning arc plasma modelling

The use of plasma simulations incorporating the conical electrode and anode, replicating the previously discussed experimental arrangement, potentially enables the electric test conditions to be input parameters and resulting specimen loading conditions to be calculated and not assumed. The majority of works modelling plasma have been focussed on gas tungsten arc (GTA) welding processes or general free burning arcs [13]–[19]. Traidia and Roger [20] produced the most appropriate model for adaption to the standard arrangement of lightning strike testing. Thus the fundamental principles and boundary conditions proposed by Traidia and Roger [22] can be traced to the latest generation of lightning plasma

modelling works. In particular, four groups of workers have proposed plasma simulations for artificial test lightning, modelling Waveforms A, B and C ([3]–[5], [21]). These simulations have great variation due to the difference in Waveform timescales and the modelling and solution approaches used, however MHD is used by all.

Chen et al. [4] and Wang et al. [5] used ANSYS Fluent to generate full 3D CFD based MHD models of lightning plasma for Waveforms A and C respectively. However, neither Chen et al. [4] nor Wang et al. [5] model the attachment of the lightning channel to the specimen but assume an initial temperature condition representing a formed plasma channel. This approach follows other plasma models in the GTA domain [22], [23], assuming a formed plasma channel and an assumed initial electrical conductivity. The models enable the calculation of the specimen loading conditions for the defined plasma, based on the applied Waveform input current. Abdelal and Murphy [3] employ a FE based MHD simulation approach to model Waveform B and attempt to predict plasma initial attachment to the specimen. The Waveform B plasma model used the Waveform electric current profile as an input with the simulation predicting plasma fluid properties and specimen (anode) surface loads. Significantly, Abdelal and Murphy [3] used a 1D electron transport model to predict air electric conductivity reducing the assumptions required and enabling the prediction of the lightning plasma channel local attachment to the specimen. Abdelal and Murphy [3] noted that for a full scale Waveform B FE based MHD simulation the expected runtime could be 70 days even with parallelisation and High Performance Computing (HPC) resources. Therefore, these authors employed a scaling approach using similitude theory. Similitude theory employs similarity between parameters using scaling factors and assumes equivalent similarity conditions between the scaled and full-scale model [3].

All of the above authors model a copper conical tip cathode while Abdelal and Murphy and Wang et al. modelled a copper specimen for the anode. Chen et al. was the only author to model a composite anode. In addition, Abdelal and Murphy [3] in their initial 1D electron transport model also modelled a copper anode but did not consider the impact of this representation on the initial conditions for the full plasma simulation. In summary, a benefit of modelling the lightning plasma is the removal of assumptions around the loading conditions on the specimen. However, the effect of specimen

representation is unknown since in each preceding work the authors have used different representations along with different solution and modelling approaches and test waveforms.

2.3 Specimen thermal-electric modelling

Damage models have shown clear variation in damage shapes and depths depending on the design of the specimen [10], [24], [25]. Various methods have been used to apply the loads to the surface including finite and expanding radii but in the vast majority of cases the loading has been assumed to match the externally applied test waveform current loading [11], [24], [26]–[29]. Abdelal and Murphy [24] modelled a composite laminate with and without a 0.05mm copper mesh Lightning Protection System (LPS), exposed to Waveform D and used temperature dependent material properties. Lee et al. [25] compared thermal damage and depth for unprotected, copper mesh protected and specimens with pitch carbon fibre paper (PCFP) protection. All authors found that the addition of protective layers changed the damage shape and area due to their relative differences in electrical conductivity. Foster et al. [26] also considered arc expansion with circular and elliptical expanding representations. All these models have typically used the same material data set for the plies and boundary conditions, with zero electrical potential at the bottom and side surfaces of the specimen.

Two authors have attempted to capture the plasma loading conditions and represent this in their damage predictions [4], [30]. Chen et al. coupled their Waveform A plasma model to a 500 x 250 mm thermal-electric model using a volume spline function after testing seven interpolation methods. From their simulation the authors were able to predict damage depth by linking predicted ply temperatures to temperatures at which initiation and completion of material decomposition and ablation occurs. In a similar vein Millen et al. [30] proposed a method to translate the loads to the test specimen's surface and apply a load set (pressure and heat flux) from a plasma model. Millen et al. demonstrated the method for a Waveform B test arrangement, again predicting damage but in this case considering a copper anode in the plasma model and a composite specimen in the damage model.

A key question not discussed within these works is the effect of test specimen representation on the prediction of the plasma behaviour. Profiles of current density, temperature, pressure and velocity have been presented at the specimen surface assuming copper or composite specimen properties. However, there is no literature on the impact of the specimen properties on the predicted plasma properties, and the resulting impact on the predicted specimen damage. This work will attempt for the first time to establish the relationships linking specimen representation, plasma properties and surface loads and the resulting specimen damage.

3.0 Methodology

As summarised in the preceding section only simulation of Waveform B has achieved modelling of the attachment behaviour of the plasma channel with the test specimen [3]. This is due in part to the relatively low magnitude of the peak current associated with this waveform and the long duration and slow rate of change of the current load [2]. Together these characteristics have prompted the most advanced modelling work on this single waveform. However, to the best knowledge of the authors no experimental damage results have been presented in literature corresponding to this current simulation state of the art, a single Waveform B strike (813/2340μs, 4kA; where T1/T2μs, I_{max}kA). However, to model another waveform with an assumed initial temperature condition, representing a formed plasma channel, would fail to enable appropriate study of test specimen representation and the resulting impact on the formation of the lightning plasma. Thus it is necessary to focus on Waveform B but to also extrapolate preceding experimental work to aid in the verification of the predicted behaviour.

Herein the plasma simulations will represent the test arrangement of Hirano [7]. An identical modelling approach to Abdelal and Murphy [3] will represent the test arrangement and thus a 2D-axisymmetric model is used with a simulation domain with a 12.5 mm radius. The simulation employs MHD and similitude theory to generate a scaled simulation of the experimental setup. Full modelling details are presented in reference [3], and are not repeated herein for brevity. In summary the Navier-

Stokes equations, Maxwell equations and the thermal conduction equations governed fluid motion, electromagnetism and heat transfer. The governing equation, representing the electric test loading condition is given by:

$$I'(t) = \frac{11300}{d\beta}\left(e^{-700\cdot t'\cdot\gamma} - e^{-2000\cdot t'\cdot\gamma}\right) = 113\left(e^{-70\cdot t'} - e^{-200\cdot t'}\right) \quad (1)$$

where γ=1e-4, β=1e8 and d=2.

3.1 Simulation test cases

Three specimen representations are considered along with the reference simulation case of Abdelal and Murphy [3]:

- Reference Case – The specimen is modelled with copper properties throughout,
- Case 1 – The specimen is modelled with epoxy properties throughout,
- Case 2 – The specimen is modelled with composite properties throughout,
- Case 3 – The specimen is modelled with a thin copper surface layer with boundary conditions adjusted to represent a surface embedded copper LPS mesh.

Case 1 represents a full epoxy specimen to provide a distinct contrast in material properties with the reference case. Case 2 represents a specimen with composite material properties, to match those used in the thermal-electric simulations, to replicate an unprotected specimen. The material properties used in each case are presented in Table 1 and all four cases can be viewed graphically in Figure 2.

Case 3 modified the reference case, to better replicate a copper mesh in a real specimen. Initial results of the preliminary simulation work, the reference case, showed the temperature rise in the thermal-electric simulation to be minimal. This was due to a low current density extracted from the specimen surface caused by very high copper electrical conductivity to ground and out of the system. Another cause was unrepresentative behaviour, coupling a copper anode in the plasma simulation to a composite specimen in the thermal-electric simulation. Such boundary conditions do not accurately

replicate the experimental test arrangement [7]. In a protected specimen the ground boundary condition would be at the bottom of the specimen, separated from the copper mesh by the composite plies. In Case 3 the depth of the copper layer was reduced to 0.05 mm and the ground boundary condition on the surface *f-e* was removed, Figure 3. The ground boundary, as shown in Figure 3, at point *d* was maintained as beyond this point (12.5 mm) further copper would exist up to the edge of the specimen and current flow would be expected to occur in this direction. However, on the bottom edge, the copper will be adjacent to the composite plies, and thus in this new case the ground boundary condition is not applied on this edge.

No modifications were made to the depth of the specimen in Cases 1 or 2. All other boundary conditions were maintained constant throughout all cases and the same mesh was used. All simulations were completed locally on a 16 core, Intel Xeon 3GHz workstation with 32GB of RAM and took around ten days to complete.

3.2 1D electron transport model

Before undertaking the test cases, as outlined in section 3.1, it is necessary to examine the behaviour of the previously developed 1D electron transport model, Figure 3, to determine if the modelled specimen properties impact the initial electron transport behaviour and the predicted electric conductivity for air. In order to test the effect of the test specimen material, the species concentration equation, Equation 2, was varied by using a scale factor, *R*, between 0 and 1.

$$C_{0,ne} = R \times n_e \tag{2}$$

Where $C_{0,ne}$ is the concentration (mol/m^3) and n_e is the electron density (1/m^3). A value of 1 represents total absorption of the incident wave of electrons in a specimen equivalent to copper while numbers less than 1 model electron accumulation at the surface, with a value of 0 representing zero electron absorption and the behaviour of an insulating material. Four tests were initially simulated with *R* values of 0, 0.1, 0.5 and 1 to determine the sensitivity of the modelling approach to anode material properties and appropriate values for the planned test cases.

3.3 Thermal-electric damage modelling

Once the plasma simulations were complete the results were passed to a set of ABAQUS thermal-electric simulations, using an incremental development of the coupling approach developed and demonstrated in reference [30]. The selected coupling approach structures the surface mesh of the thermal-electric damage model to enable the MHD predicted current density to be applied with minimal approximation. The thermal-electric simulations modelled the experimental arrangement with a composite specimen measuring 150 × 100 mm and containing 32 plies giving a total thickness of 4.704 mm. The specimen was modelled with a ply layup of $[45/0/-45/90]_{4s}$ and the material properties of IM600/133 (replicating the specimen design of Hirano [7] and selected to support with model verification and prediction interpretation, section 3.4). In all analyses a transient, fully coupled, thermal-electric step was used with DC3D8E elements [31].

Temperature dependent material properties were used in all analyses. The same zero electrical potential boundary condition was applied to the side and bottom surfaces of the specimen, as with the plasma simulation anode, to replicate experimental conditions [7]. In Case 1 a 0.05mm epoxy layer was included above the top ply with the properties shown in Table 2. The model assumed an initial electric conductivity until the onset of material decomposition, during decomposition the electrical conductivity was assumed to increase linearly, at 800°C the epoxy was assumed to ablate and above this temperature a fully conductive value of electric conductivity was modelled ($1x10^6$ 1/ Ω.mm). This relationship was based on TGA experiments within literature for epoxy [32]–[34]. In this case the energy released during resin decomposition was the same as that used for the unprotected laminate. Case 2 was a standard unprotected laminate and the properties are shown in Table 3. In Case 3 a 0.05mm copper mesh was placed on top of the plies with properties shown in Table 4. In all circumstances the simulation mesh was converged using the same temperature contour size criteria as applied in previous works[26]. This resulted in a total element count of 45,670, 43,718 and 70,680 elements respectively for Cases 1, 2 and 3. ABAQUS user subroutines UMATHT, HETVAL and USDFLD were used to define the thermal

behaviour of the material, model decomposition and update material properties respectively, replicating the approach used by Abdelal and Murphy [24] and Foster et al. [26].

3.4 Verification data

In order to support the interpretation of the simulation results and assess their validity it is appropriate to explore the available experimental data. Kindly provided by Hirano [7], Table 5 presents six test damage profiles for equivalent unprotected specimens subjected to varying loading. This data is used to create some general approximations of the likely damage resulting from a single Waveform B strike.

First applying the same image binarisation and characterisation method proposed by Foster et al. [26] for moderate and severe damage (where moderate damage - is defined as a wide surface area with thermal decomposition and sharp and shiny resin; severe damage - defined by a deeper area penetrating multiple plies with char residue) it is possible to plot the damage areas against the waveform parameters of T1, T2 and peak current. Figure 4 presents example measurements of moderate and severe damage. Based on the generated experimental data, regression and forecasting can be performed for different waveforms. A single forecast, based on peak current, is presented for Waveform B in Table 4. The peak current forecast is selected due to the extreme difference in T1/T2 values between Waveforms A and B. Such a forecast is a gross simplification and is not expected to be extremely accurate, for example as it does not consider the non-linear relationship between the impedance of the specimen and the applied current as determined from the experimental work of Sun et al. [35]. However, the forecast will prove useful as an initial order of magnitude assessment of the simulation predictions, given the current lack of experimental data. The forecast Waveform B moderate damage area is 107% of the measured value of Hirano's specimen B-4, Figure 4, and 118% of the C-3 value. The projected severe damage area is 41% of B-4 and 81% of C-3, Table 5 and Figure 4. These values are discussed in the following results section along with the case test simulation results.

4.0 Results

First the behaviour of the 1D electron transport model is presented. This is followed by the four case study results. First the overall plasma behaviour is considered (covering pressure, velocity, temperature and current density within the plasma domain – referencing Figure 2 and Table 6). Secondly the predicted specimen surface loading is discussed with paying particular attention to the current density on the surface as this was passed to thermal-electric models (Figure 2, Table 6 and Figure 6). Finally, temperature contours and damage plots will be presented for the thermal-electric simulations and used to discuss the resultant damage (focusing on the damage surface area, depth and volume, also summarised in Table 6).

4.1 1D Electron transport model results

Plotting predicted electrical conductivity for the 1D Electron transport model with varying electron absorption scale factors (*R* values of 0, 0.1, 0.5 and 1) it can be observed that the species concentration at the anode surface has a negligible effect on the predicted initial electrical conductivity of the air, Figure 5. The total variation in the time for the conductivity to reach a value of zero is 0.51 ms.

Given the limited sensitivity observed a single scale factor value (R=1) is thus used for each of the test case simulations. These results, indicating a general insensitivity, allow the case study simulations to vary only mechanical, electrical and thermal material properties associated with the specimen.

4.2 Specimen representation

4.2.1 General observations of physics occurring during simulations

Generally all simulations begin in the same manner. A large accumulation of current within the cathode is discharged and forms an arc between the cathode and the specimen, governed by the results of the 1D model, before beginning to expand. Expansion begins at approximately 0.394 ms which corresponds to the time at which the initial electrical conductivity, generated by the 1D model, falls to zero. Up to

this point pressure is constant at both surfaces. The pressure initially falls to approximately 0.08 MPa before rising to 0.14 MPa and returning to around 0.1013 MPa at both the cathode and specimen. Expansion continues up to waveform peak with more current entering the system before decreasing in line with the incident waveform profile. However, due to heat transfer and propagation of the pressure wave both temperature and pressure contours continue to expand. Moreover, by 2.5 ms, the T2 time of waveform B, all simulations converge to a stable pressure of 0.1013 MPa at the cathode and specimen respectively, a return to the initial conditions and only a 0.2% difference between cathode and specimen pressure. Although the temperature and pressure contours continue to expand their rate of change is reduced because the velocity profile follows that of the incoming current load.

4.2.2 Plasma behaviour due to specimen representation

Focussing firstly on the current density within the plasma, Table 6, a clear pattern emerges between the results with highly conductive specimens, copper, and without, composite or epoxy. The reference case has a 26% lower plasma current density than Case 1 which in turn is 0.21% higher than that of Case 2.

Comparing peak pressures in the plasma, Case 3 predicts the highest pressure and Case 2 the lowest, however the maximum difference in peak pressure for all four cases is less than 10%. Figure 2 illustrates the general pressure wave pattern, plotting the pressure contour at the time when the peak current is applied.

Focusing on the velocity, Table 6, the maximum difference in peak velocity for all four cases is less than 1%. Case 3 has the highest waveform peak velocity and the reference case has the lowest peak velocity. This illustrates an inverse relationship between specimen thickness and peak plasma velocity.

Finally looking at plasma temperature it can be seen that once again the maximum variation between cases is less than 1%. Case 2 shows some increase in temperature in the specimen itself but this is less significant than is predicted in Case 1 - due to the improved electrical and thermal

conductivity in the reinforced polymer specimen. This behaviour is confirmed by examining Table 6 where the surface temperature for Case 2 falls between the reference case and Case 1 at *time=1ms.*

4.2.3 Specimen surface loads due to specimen representation

Focussing on the surface loads the specimen material or design has a more pronounced effect on results. Firstly focussing on the specimen surface pressure, Figure 2, in Cases 1 (highest, peak of 0.113 MPa) and 2, the specimen surface pressure follows the trend of the applied waveform, with the predicted pressure rising as the applied current increases, and then dropping after the peak current, ultimately returning to the original atmospheric pressure by the end of the waveform application. However, neither the reference case (lowest trough of 0.076 MPa) nor Case 3 pressures follow this trend. In these cases the specimen surface pressure remains around atmospheric throughout the entire application of the current waveform. For all specimen representations the line plots show that the general trend of pressure is similar with only minor variations in the local magnitudes and peak and trough timings.

The maximum difference in velocity at waveform peak between cases at the specimen surface is 68%. Case 1 surface velocity is higher than Case 2 due to the lowest density of the three materials and an extremely low electrical conductivity related to velocity through Maxwell's equations and the fluid flow equations within the model. Case 2 and the reference case have very similar surface velocity magnitudes, being identical at *time=1ms*. The Case 2 and reference velocities are generally 28% smaller in magnitude than that predicted in case study 3 at equivalent locations and times. The key parameters effecting the velocity of the plasma are the electrical and thermal conductivity of each specimen as noted in the experimental work of Sonehara et al. [36].

The surface temperature of the specimen rises following the same trend for all cases, with the highest temperature where the centre of the plasma channel meets the specimen. The surface temperature falls steadily from this central position, consistently reaching room temperature at a radial distance from the centre of approximately 4 mm, Figure 2. The peak surface temperature is lowest for

the reference case however; Case 3 is only 9% greater due to the improved thermal and electrical conductivity of the copper which results in superior heat dissipation and current flow to ground. The largest temperature occurs in Case 1, which is 26% greater than the peak of Case 2, which in turn is 273% higher than the reference case peak surface temperature. This is further supported by observing the surface current density, Table 6.

In the reference case current flow to ground is high which reduces the accumulation of the current at the surface. In Case 1 the accumulation is larger due to the lower electrical conductivity of epoxy compared with copper. Figure 6 shows how the current flow path differs between the individual cases. In the reference case there is a clear conductive path to ground throughout the specimen in both the *r* and *z* directions. However, in Cases 1 and 2 the major current flow is in the *r* direction except for a small amount of *z* direction flow beneath the attachment location of the plasma channel on the specimen. In Case 3, while current can penetrate the entire specimen the flow path is predominately in the *r* direction due to the edge ground boundary condition and the insulating properties of the composite plies and thus the absence of an efficient route to ground in the *z* direction.

Looking at the current density at the specimen surface the behaviour of Cases 1 and 2 are identical. This is again down to the relatively poor electrical conductivity compared with the reference case. Despite Case 2 having high electrical conductivity in the *r* direction, the axi-symmetric nature of the model and the ground boundary conditions result in a similar current flow through the specimen to ground in spite of the change in material properties.

The influence of ground boundary conditions can be observed by looking at Case 3 in more detail. The current density in Case 3 matches Cases 1 and 2 with a much higher peak than the reference case, Table 6. This representation is more realistic as the experimental boundary conditions are more precisely represented. In fact the Case 3 current profile is close to the profile at the bottom surface, surface *f-e*, of the reference case. However, in the reference case the magnitude is marginally smaller due to a flow of current out of the ground boundary condition on the surface *d-e*. The Case 3 surface velocity, Table 6, reinforces the earlier observation about velocity and electrical conductivity. Since the

depth of the copper layer is smaller the time taken for current to flow through to the boundary is smaller. Surface temperature, Table 6, also shows a minimal increase when compared with the reference case.

Summarising the results of the four plasma simulations it can be observed that for a highly thermally and electrically conductive material the pressure and temperature at the specimen surface are much lower than the poorly conducting materials. This is despite Case 2 having a high electrical conductivity in the *r* direction. This type of axisymmetric simulation and the positioning of the ground boundary conditions place a strong reliance on through-thickness conductivity to dissipate the current load to the ground. This observation is clear when looking at the reference case and Case 3 where the reduced depth of the conducting path and the positioning of the ground boundary conditions has changed the current density profiles on the specimen surface significantly.

The thermal-electric damage predictions for the four case studies will now be discussed.

4.4 Damage results from thermal-electric simulations

A comparison of the extent of damage on each specimen will now be presented. Case 1 and 2 will be discussed individually, using plots of the removed elements representing severe damage, and compared to the experimental damage trends in Figure 4 and Table 5. Case 3 will be compared with the results for the reference case using temperature contour plots due to the reduced damage volumes and areas. A summary of all predicted damage properties (severe and moderate damage – total volume, damage surface area, damage depth) is provided in Table 6.

4.4.2 Case 1 – Epoxy

The full extent of severe damage for this simulation is shown in Figure 8, while temperature contours for each ply are provided in Figure 9. Overall damage is large with a focus on the centre of the specimen. Due to being a poor conductor the top layer of epoxy does little to prevent composite specimen thermal

damage. The path of least resistance is down into the composite plies rather than outward through the top epoxy layer to the zero potential boundary condition at the plate extremities. This results in a larger damage area at the centre of the top ply (ply 1) and a smaller amount of damage at the specimen extremities. The reduction in energy passing to lower plies allows the current more time to flow towards the edges of the specimen as seen in plies 4 and 5 where the 300°C contour has reached these points. Once the epoxy layer passes 300°C the electrical conductivity increases in all directions (representing the decomposition of the epoxy material) hence the similarity in shape between the top epoxy layer and the 500°C contour on ply 1. The area of the 300/500°C temperature contours on ply 1 is 3342/1027 mm^2 while moderate/severe damage volumes are 2531/810 mm^3 respectively, Table 6. Interestingly these predicted areas are larger than those predicted by Foster et al. [26] for a circular expanding arc under reduced peak magnitude Waveform A loading (4/20μs, 40kA). Foster et al. predicted surface 300/500°C contours of 3218/450 mm^2. Comparing the Case 1 prediction with the extrapolated Waveform B experimental results (3555/400 mm^2, Table 5) it can be seen that the moderate damage is similar but the severe damage area is predicted to be significantly larger. The run time for this thermal-electric simulation was 52 hours compared with 10 days for the plasma simulations.

4.4.3 Case 2 – Composite

The full extent of severe damage for Case 2 is shown in Figure 8, while temperature contours for each ply are provided in Figure 10. The surface damage takes on the typical elongated profile due to the zero electrical potential boundary conditions. In this case damage extends to 13 plies deep (1.91mm) and the area of the 300/500°C temperature contours on the top ply are 3661/1372 mm^2. Moderate and severe damage volumes are 2082/726 mm^3 respectively as outlined in Table 6. When compared with Case 1 it can be seen that both moderate and severe damage areas are larger for Case 2 by 10% and 34% respectively. However, the damage volume is smaller as more current has flowed to ground on the top ply of the composite specimen. The difference in damage areas and depth are notably larger in magnitude than the difference in instantaneous plasma properties seen in Table 6 and Figure 2, indicating that the modelling of the specimen within the plasma simulation does significantly influence

damage prediction. These values are also different from the results of previous works for the reduced peak magnitude Waveform A [4], [26] and significantly larger than those for the reference case. The reference case results are presented in Figure 7 and Table 6 and summarised as: moderate surface damage area of 259 mm^2, extending to one ply deep (0.147mm). The unprotected specimen in Case 2 has a 1200% deeper damage penetration and 1314% larger damage area when compared to the reference case.

In the case of Waveform B the current loading rate is comparatively small when compared with Waveform A. However, the 100 times longer exposure to current loading provides greater opportunity for resistive heating. Comparing this with experimental work, the observations from Hirano's work was that as the duration of the Waveform increased and the peak current decreased, the resin deterioration area and the amount of charring increased, as shown in the two experimental results presented in Figure 4 [7]. Also, the severe damage area is much larger (243%) than that forecast based on the preceding experimental work but the moderate damage area prediction is within 3% of the forecasted value shown previously in Table 5. Damage depth is also largest in the unprotected Case 2 at thirteen plies compared with one in the reference case and eight in Case 1. The run time for this simulation was 41.5 hours.

4.4.4 Case 3 – Copper

Case 3 features a 0.05mm copper mesh layer on the top surface of the specimen. In this case a temperature rise of 55°C is predicted in the first ply layer, well below that which would cause significant damage to the composite material. However, this peak temperature is 50°C greater than that predicted in the reference case. This is in spite of Case 3 having over eight times higher peak current density on the specimen surface, predicted by the plasma model, Figure 2. The run time for this simulation was 85 hours and the thermal damage profile is shown in Figure 7. Both of these cases have noted damage areas but these are confined to the copper mesh layer and reference the temperature to cause composite ply damage, 300°C. These results would suggest that for Waveform B a copper protection system is more than capable of dispersing the current effectively to minimise damage and temperature rise in the

underlying plies. This is due to the high conductivity of the copper layer and the ability of the layer to dissipate the incident current at a rate greater than which it is being applied. Accumulation of current on the surface occurs in both Cases 1 and 2 with a slower dispersal rate and therefore larger damage areas.

4.4.5 Summary of observed damage

The difference in electrical conductivity between Case 3 and the other cases is crucial for managing the amount of damage incurred. The conductivity of the copper layer is 1600 times greater than in the composite fibre direction. This means that the copper layer can dissipate the incident current at a rate greater than it is being applied while in Cases 1 and 2 the lower conductivity means that current is being applied at a greater rate than can be dissipated and for a longer time period. Damage is therefore greater for both the epoxy and unprotected specimens. In both of these simulations there is a volume of elements still present at the centre of the specimen, behaviour not observed in experiments. This suggests that there are other physics involved and not captured within these simulations.

5.0 Conclusions

This paper presents a comparison of the plasma generated and thermal damage produced during an artificial lightning strike using test Waveform B, analysing the effect of specimen representation. Four specimens were compared with the effects on plasma properties observed. These effects were minimal with the maximum difference within the plasma being 1%. The surface load predictions vary with the representation of the specimen properties within the plasma model, with surface pressure and temperature reducing with increasing specimen conductivity. In particular, changing the specimen representation from copper to epoxy increased the surface current density load by a factor of eight. This

finding is intuitive, however herein the effect is quantified for the first time. The influence of specimen representation has a much larger effect on the prediction of specimen thermal damage, with order of magnitude changes in damage depth and surface area witnessed within the range of simulation case studies. The simulation case studies have also demonstrated the behaviour of a surface copper protective layer effectively eliminating thermal damage. This work has also presented a full prediction of damage for an unprotected specimen loaded with Waveform B. These results suggest that thermal decomposition is more prevalent for Waveform B than the reduced magnitude Waveform A typically used as an experimental reference in the simulation literature. This effect is due to long exposure to the current and the opportunity for greater resistive heating despite a lower peak current. These observations are supported by experimental findings at longer durations and lower peak currents and the simulation results compare favourably with the extrapolated moderate damage results from preceding experimental tests. Future work should modify the test Waveform to analyse the effects on plasma and damage. The current work has been sequentially coupled due to computational cost. Future work should also develop improved and less expensive Finite Element-MHD and Finite Volume-MHD models including initial attachment and plasma-surface interactions and incorporate more of the key physics to eliminate the volume of elements still present at the centre of the specimen.

Acknowledgements

The authors would like to thank The Engineering and Physical Sciences Research Council (EPSRC) for funding this work as part of the PhD research of S. Millen.

References

[1] S. Eliezer and Y. Eliezer, *The Fourth State of Matter - An Introduction to Plasma Science*, 2nd ed. Bristol: Institute of Physics Publishing, 2001.

[2] SAE Aerospace, “Aerospace Recommended Practice ARP5412B,” 1999.

[3] G. F. Abdelal and A. Murphy, "A multiphysics simulation approach for efficient modeling of lightning strike tests on aircraft structures," *IEEE Trans. Plasma Sci.*, vol. 45, no. 4, pp. 725–735, 2017.

[4] H. Chen, F. S. Wang, X. T. Ma, and Z. F. Yue, "The coupling mechanism and damage prediction of carbon fiber/epoxy composites exposed to lightning current," *Compos. Struct.*, vol. 203, no. December 2017, pp. 436–445, 2018.

[5] F. Wang, X. Ma, H. Chen, and Y. Zhang, "Evolution simulation of lightning discharge based on a magnetohydrodynamics method," *Plasma Sci. Technol.*, vol. 20, no. 7, 2018.

[6] P. Feraboli and M. Miller, "Damage resistance and tolerance of carbon/epoxy composite coupons subjected to simulated lightning strike," *Compos. Part A Appl. Sci. Manuf.*, vol. 40, no. 6–7, pp. 954–967, 2009.

[7] Y. Hirano, S. Katsumata, Y. Iwahori, and A. Todoroki, "Artificial lightning testing on graphite/epoxy composite laminate," *Compos. Part A Appl. Sci. Manuf.*, vol. 41, no. 10, pp. 1461–1470, 2010.

[8] H. Kawakami, "Lightning Strike Induced Damage Mechanisms of Carbon Fiber Composites," Washington, 2011.

[9] P. Feraboli and H. Kawakami, "Damage of Carbon/Epoxy Composite Plates Subjected to Mechanical Impact and Simulated Lightning," *J. Aircr.*, vol. 47, no. 3, pp. 999–1012, 2010.

[10] F. S. Wang, Y. Y. Ji, X. S. Yu, H. Chen, and Z. F. Yue, "Ablation damage assessment of aircraft carbon fiber/epoxy composite and its protection structures suffered from lightning strike," *Compos. Struct.*, vol. 145, pp. 226–241, 2016.

[11] S. Kamiyama, Y. Hirano, and T. Ogasawara, "Delamination analysis of CFRP laminates exposed to lightning strike considering cooling process," *Compos. Struct.*, vol. 196, pp. 55–62, 2018.

[12] R. Muñoz, S. Delgado, C. González, B. López-Romano, D. Y. Wang, and J. Llorca,

"Modeling lightning impact thermo-mechanical damage on composite materials," *Appl. Compos. Mater.*, vol. 21, no. 1, pp. 149–164, 2014.

[13] H. G. Fan, Y. W. Shi, and S. J. Na, "Numerical analysis of the arc in pulsed current gas tungsten arc welding using a boundary-fitted coordinate," *J. Mater. Process. Technol.*, vol. 72, pp. 437–445, 1997.

[14] F. Lago, J. J. Gonzalez, P. Freton, and A. Gleizes, "A numerical modelling of an electric arc and its interaction with the anode: Part I. The two-dimensional model," *J. Phys. D. Appl. Phys.*, vol. 37, no. 6, pp. 883–897, 2004.

[15] F. Lago, J. J. Gonzalez, P. Freton, F. Uhlig, N. Lucius, and G. P. Piau, "A numerical modelling of an electric arc and its interaction with the anode: part III. Application to the interaction of a lightning strike and an aircraft in flight," *J. Phys. D. Appl. Phys.*, vol. 39, no. 10, pp. 2294–2310, 2006.

[16] M. Tanaka, H. Terasaki, M. Ushio, and J. J. Lowke, "A Unified Numerical Modeling of Stationary Tungsten-Inert- Gas Welding Process," *Metall. Mater. Trans. A*, vol. 33, no. July, pp. 2043–2052, 2002.

[17] M. Tanaka and J. J. Lowke, "Predictions of weld pool profiles using plasma physics," *J. Phys. D. Appl. Phys.*, vol. 40, pp. R1–R23, 2006.

[18] L. Sansonnens, J. Haidar, and J. J. Lowke, "Prediction of properties of free burning arcs including effects of ambipolar diffusion," *J. Phys. D. Appl. Phys.*, vol. 33, no. 2, pp. 148–157, 1999.

[19] J. J. Lowke, R. Morrow, and J. Haidar, "A simplified unified theory of arcs and their electrodes," *J. Phys. D. Appl. Phys.*, vol. 30, no. 14, pp. 2033–2042, 1997.

[20] A. Traidia and F. Roger, "Numerical and experimental study of arc and weld pool behaviour for pulsed current GTA welding," *Int. J. Heat Mass Transf.*, vol. 54, no. 9–10, pp. 2163–2179, 2011.

[21] L. Chemartin, P. Lalande, B. Peyrou, A. Chazottes, P. Q. Elias, C. Delalondre, B. G. Cheron, and F. Lago, "Direct Effects of Lightning on Aircraft Structure : Analysis of the Thermal , Electrical and Mechanical Constraints," *J. Aerosp. Lab*, no. 5, pp. 1–15, 2012.

[22] H. G. Fan and Y. W. Shi, "Numerical simulation of the arc pressure in gas tungsten arc welding," *J. Mater. Process. Technol.*, vol. 61, pp. 302–308, 1996.

[23] C. S. Wu and J. Q. Gao, "Analysis of the heat flux distribution at the anode of a TIG welding arc," *Comput. Mater. Sci.*, vol. 24, pp. 323–327, 2002.

[24] G. F. Abdelal and A. Murphy, "Nonlinear numerical modelling of lightning strike effect on composite panels with temperature dependent material properties," *Compos. Struct.*, vol. 109, no. 1, pp. 268–278, 2014.

[25] J. Lee, T. E. Lacy, C. U. Pittman, and M. S. Mazzola, "Thermal Response of Carbon Fiber Epoxy Laminates with Metallic and Nonmetallic Protection Layers to Simulated Lightning Currents," *Polym. Compos.*, 2017.

[26] P. Foster, G. Abdelal, and A. Murphy, "Understanding how arc attachment behaviour influences the prediction of composite specimen thermal loading during an artificial lightning strike test," *Compos. Struct.*, vol. 192, pp. 671–683, 2018.

[27] Q. Dong, G. Wan, L. Ping, Y. Guo, X. Yi, and Y. Jia, "Coupled thermal-mechanical damage model of laminated carbon fiber/resin composite subjected to lightning strike," *Compos. Struct.*, vol. 206, pp. 185–193, 2018.

[28] Q. Dong, Y. Guo, X. Sun, and Y. Jia, "Coupled electrical-thermal-pyrolytic analysis of carbon fiber/epoxy composites subjected to lightning strike," *Polym. (United Kingdom)*, vol. 56, pp. 385–394, 2015.

[29] T. Ogasawara, Y. Hirano, and A. Yoshimura, "Coupled thermal-electrical analysis for carbon fiber/epoxy composites exposed to simulated lightning current," *Compos. Part A Appl. Sci. Manuf.*, vol. 41, no. 8, pp. 973–981, 2010.

[30] S. L. J. Millen, A. Murphy, G. F. Abdelal, and G. Catalanotti, "Quantifying the Influence of Plasma - Solid Mechanics Coupling on the Prediction of Lightning Strike Composite Specimen Damage," in *1st International Conference on Advances in Aerospace Structures, Systems & Technology (AASST)*, 2018, pp. 103–112.

[31] ABAQUS 2016 Documentation, *Abaqus User Subroutines Reference Guide*. 2017.

[32] P. P. Vijayan, D. Puglia, J. M. Kenny, and S. Thomas, "Effect of organically modified nanoclay on the miscibility, rheology, morphology and properties of epoxy/carboxyl-terminated (butadiene-co- acrylonitrile) blend," *Soft Matter*, vol. 9, no. 10, pp. 2899–2911, 2013.

[33] S. Ma, W. Liu, Y. Zhao, Z. Yan, and N. Gao, "Curing behavior and thermal properties of autocatalytic cycloaliphatic epoxy," *J. Macromol. Sci. Part A Pure Appl. Chem.*, vol. 49, no. 1, pp. 81–84, 2012.

[34] W. O. De Souza, K. Garcia, C. F. de A. Von Dollinger, and L. C. Pardini, "Electrical Behavior of Carbon Fiber / Phenolic Composite during Pyrolysis," *Mater. Res.*, vol. 18, no. 6, pp. 1209–1216, 2015.

[35] A. J. Sun, B. X. Yao, C. W. Xu, and D. J. Chen, "Dynamic characteristics of carbon fiber reinforced polymer under nondestructive lightning current," *Polym. Compos.*, vol. 39, no. 5, pp. 1514–1521, 2018.

[36] T. Sonehara, H. Kusano, N. Tokuoka, and Y. Hirano, "Visualization of lightning impulse current discharge on CFRP laminate," in *2014 International Conference on Lightning Protection, ICLP 2014*, 2014, vol. 4, pp. 835–839.

Table 1 - Anode material properties.

Property	Copper	Epoxy	IM600/133	Unit

Electrical Conductivity (σ)	5.998e7	1.00e-10	35971	1.15	0.00179	S/m
Heat Capacity (C_p)	385	1065	1065			J/kg.K
Density (ρ)	8700	1330	1520			kg/m^3
Thermal Conductivity (k)	400	0.79	8	0.67	0.67	W/mK
Thermal Expansion Coefficient (α)	1.7e-5	5.0e-6	1.53e-6			1/K
Young's Modulus (E)	205e9	36.2e9	130e9			Pa
Poisson's Ratio (ν)	0.28	0.389	0.3			(-)

Table 2 - Temperature dependent epoxy material properties.

Temperature (°C)	Specific Heat (J/kg°C)	Electrical Conductivity (1/ Ω.mm)	Thermal Conductivity (W/mm.K)	Density (kg/mm^3)
25	1065	$1x10^{-10}$	0.00079	$1.33x10^{-6}$
500	2100	2	0.00021	$1.33x10^{-6}$
800	2100	$1x10^{6}$	0.00012	$9.98x10^{-7}$
3316	2500	$1x10^{6}$	0.00012	$9.98x10^{-7}$
	Temperature Range (°C)		Energy Released (J)	
Resin Decomposition	500-800		$4.8x10^{6}$	

Table 3 - Temperature dependent CFRP material properties.

Temperature dependent material properties				
		Thermal Conductivity		
Temperature (^oC)	Specific Heat (J/kg^oC)	Fibre (W/mm.K)	Transverse (W/mm.K)	Through-Thickness (W/mm.K)
25	1065	0.008	0.00067	0.00067
500	2100	0.004390	0.000342	0.000342
800	2100	0.002608	0.00018	0.00018
1000	2171	0.001736	0.0001	0.0001
3316	2500	0.001736	0.0001	0.0001
3334*	5875	0.001736	0.0001	0.0001
3335*	5875	0.0005	0.0005	0.0005
7000*	5875	0.001015	0.001015	0.001015
Temperature dependent material properties				
		Electrical Conductivity		
Temperature (^oC)	Density (kg/mm^3)	Fibre (1/ Ω.mm)	Transverse (1/ Ω.mm)	Through-Thickness (1/ Ω.mm)
25	$1.52x10^{-6}$	35.97	0.001145	$1.79x10^{-6}$
500	$1.52x10^{-6}$	35.97	0.001145	$1.79x10^{-6}$
800	$1.10x10^{-6}$	35.97	0.001145	$1.79x10^{-6}$
3316	$1.10x10^{-6}$	35.97	0.001145	$1.79x10^{-6}$
3334*	$1.11x10^{-9}$	35.97	2	$1x10^6$
3335*	$1.11x10^{-9}$	0.2	0.2	$1x10^6$
7000*	$1.11x10^{-9}$	1.5	1.5	$1x10^6$
* - Gas				

	Temperature Range (^oC)	Energy Released (J)
Resin Decomposition	500-800	$4.8x10^6$
Fibre Ablation	3316-3334	$43x10^6$

Table 4 - Temperature dependent copper material properties.

Temperature (°C)	Specific Heat (J/kg°C)	Electrical Conductivity (1/ Ω.mm)	Thermal Conductivity (W/mm.K)	Density (kg/mm^3)
25	385	58140	0.401	8.95×10^{-6}
500	431	20120	0.37	1.1×10^{-6}
1000	491	4651	0.15	1.1×10^{-6}
1700	491	3704	0.18	1.1×10^{-6}
2600	491	2404	0.18	1.1×10^{-6}
7000	491	1500	0.18	1.1×10^{-6}
8000	550	1400	0.18	1.1×10^{-6}

Table 5 - Estimated damage areas from Hirano's experimental work [7].

Test Specimen	T1	T2	Peak Current (kA)	Estimated Moderate Damage Area (mm^2)	Estimated Severe Damage Area (mm^2)
A-1	2.6	10.5	40	1991	510
B-1	4	10	30	1565	108
B-4	4	20	40	3316	975
C2-1	4	20	40	2050	950
C-1	7	150	20	4047	652
C-3	7	150	10	3024	492
Waveform B (based on a linear regression)	813	2340	4	3555*	400*

*values extrapolated from experimental results.

Table 6 - Output summary for plasma and thermal-electric simulations

Case	Plasma Properties							
	Fluid (at Waveform peak)				Specimen Surface (at time = 1ms)			
	Temperature (K)	Pressure (Pa)	Velocity (m/s)	Current Density (A/mm^2)	Temperature (K)	Pressure (Pa)	Velocity (m/s)	Current Density (A/mm^2)
Reference	33,981	187,100	2057	641.6	507	107,500	22.4	5.13
1	34,042	184,770	2064	866.7	2374	112,850	31.0	43.6
2	34,043	184,410	2062	864.9	1891	110,830	22.4	43.5
3	34,040	198,260	2071	645.6	553	108,620	10.0	43.9

	Specimen Damage Summary					
	Damage Depth		Moderate Damage Area (mm^2)	Severe Damage Area (mm^2)	Moderate Damage Volume (mm^3)	Severe Damage Volume (mm^3)
	Plies	mm				
Reference	1	0.147	259	-	38.07	-
1	8	1.176	3342	1027	2531	810
2	13	1.910	3661	1372	2082	726
3	1	0.147	914	-	134.4	-

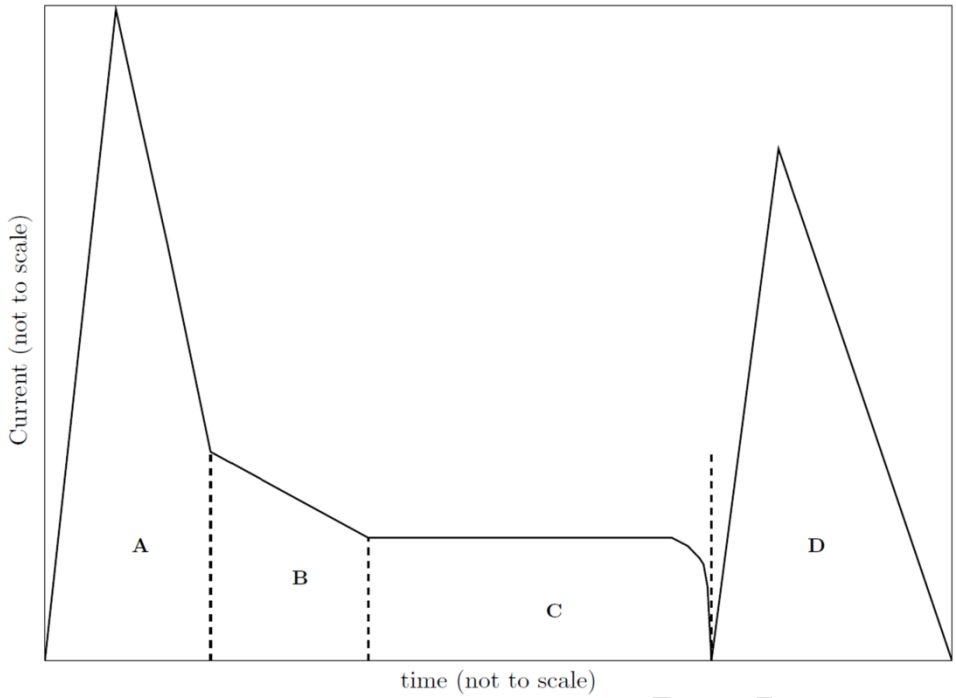

Figure 1 - Standardised lightning current waveforms.

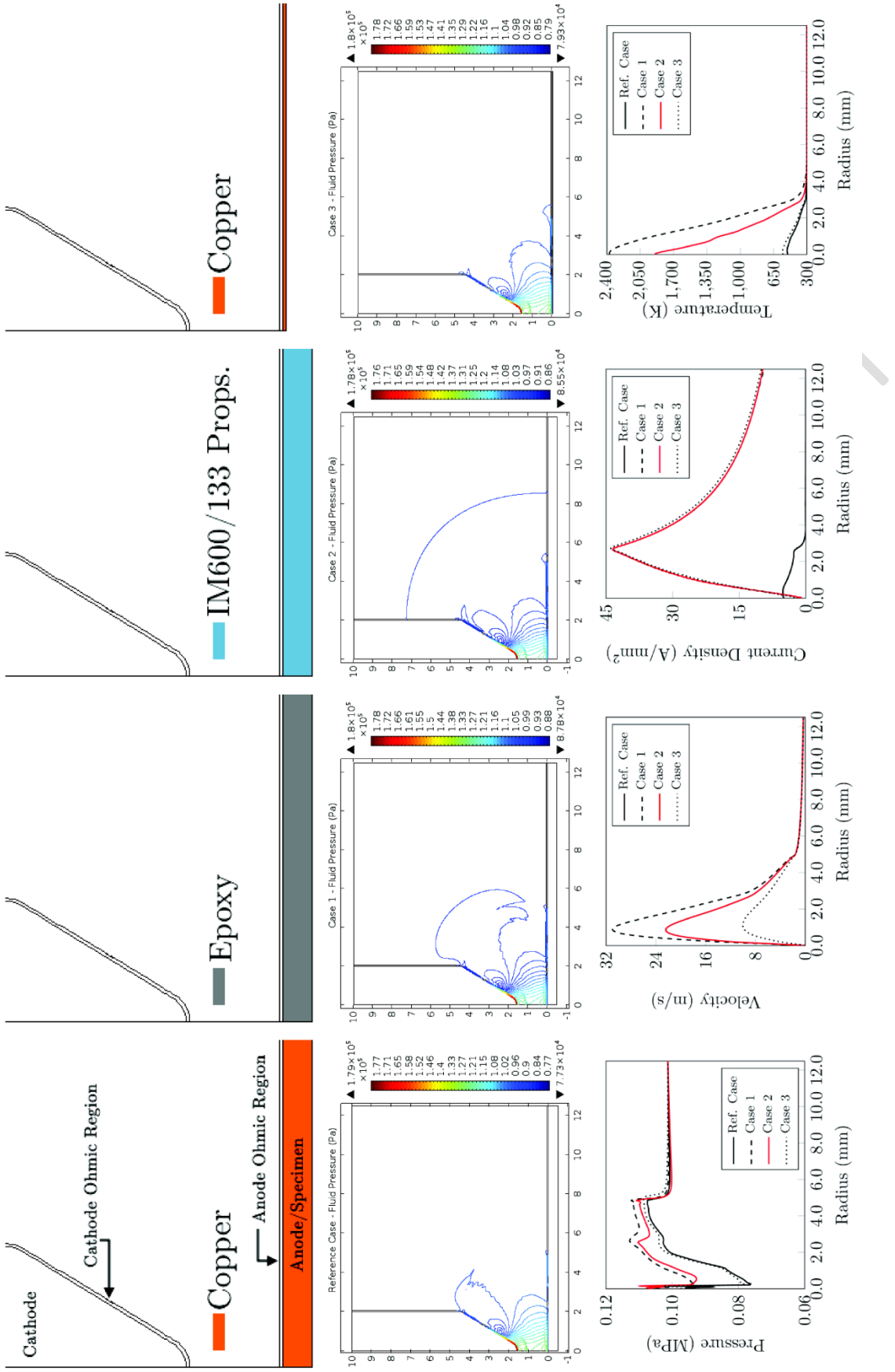

Figure 2 - Graphical representation of four test cases (top), exemplar plasma pressure contours at Waveform peak (middle) and specimen surface loads at time = 1ms (bottom).

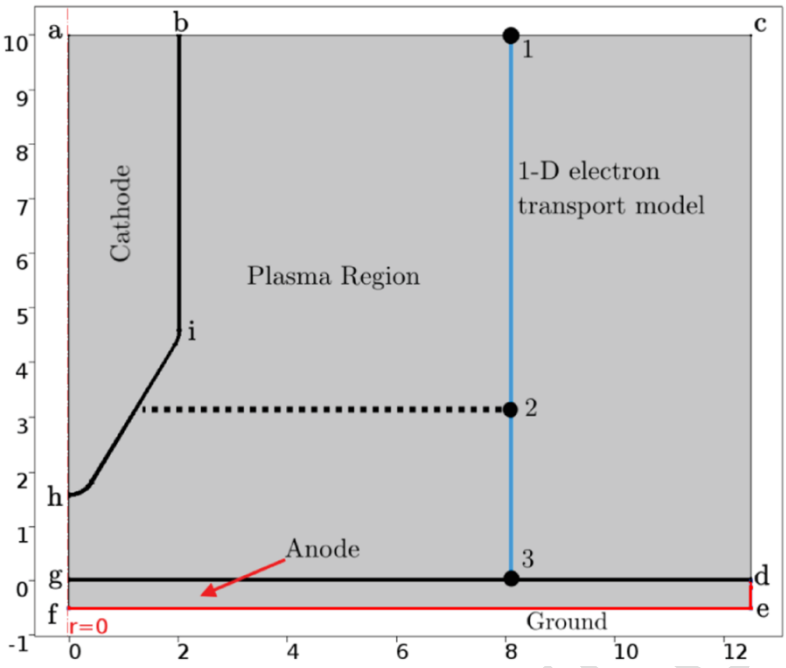

Figure 3 - Plasma and 1D electron transport simulation domains.

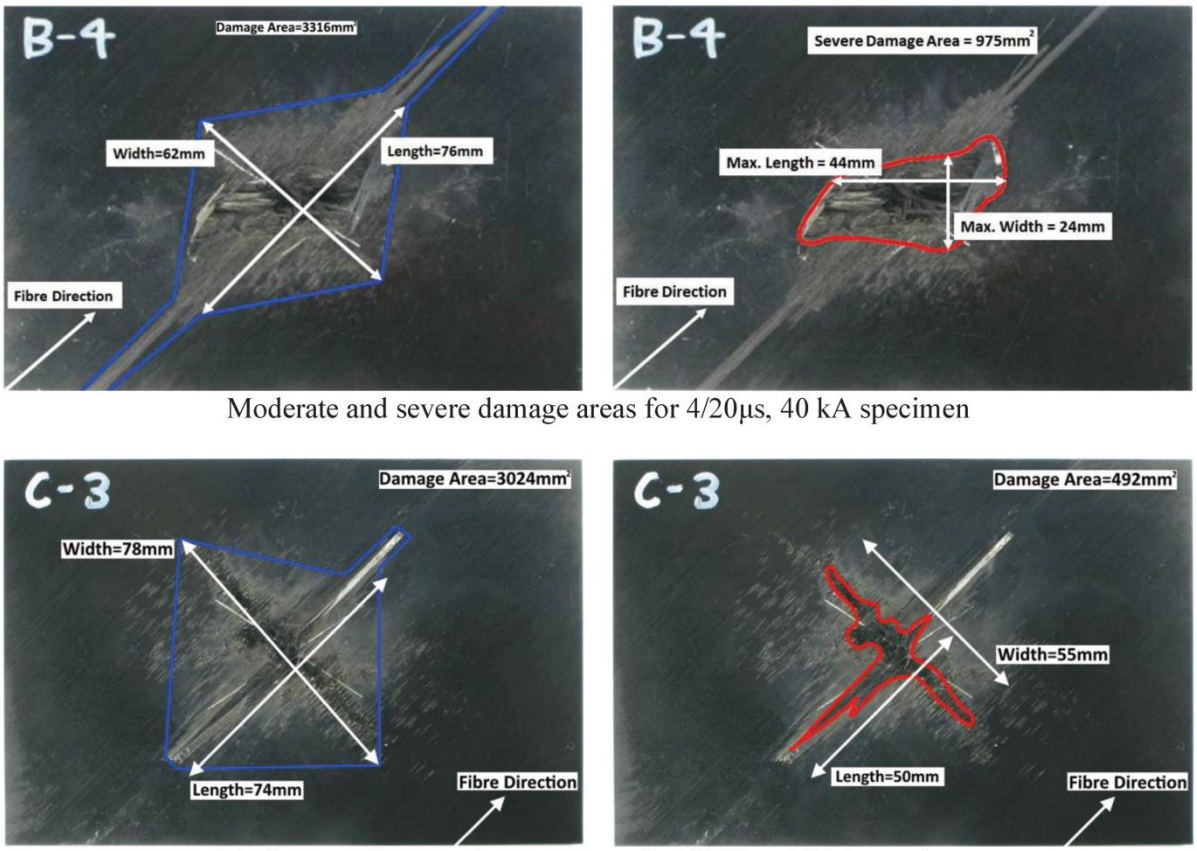

Figure 4 - Comparison of moderate and severe damage areas for different Waveforms [7], [26].

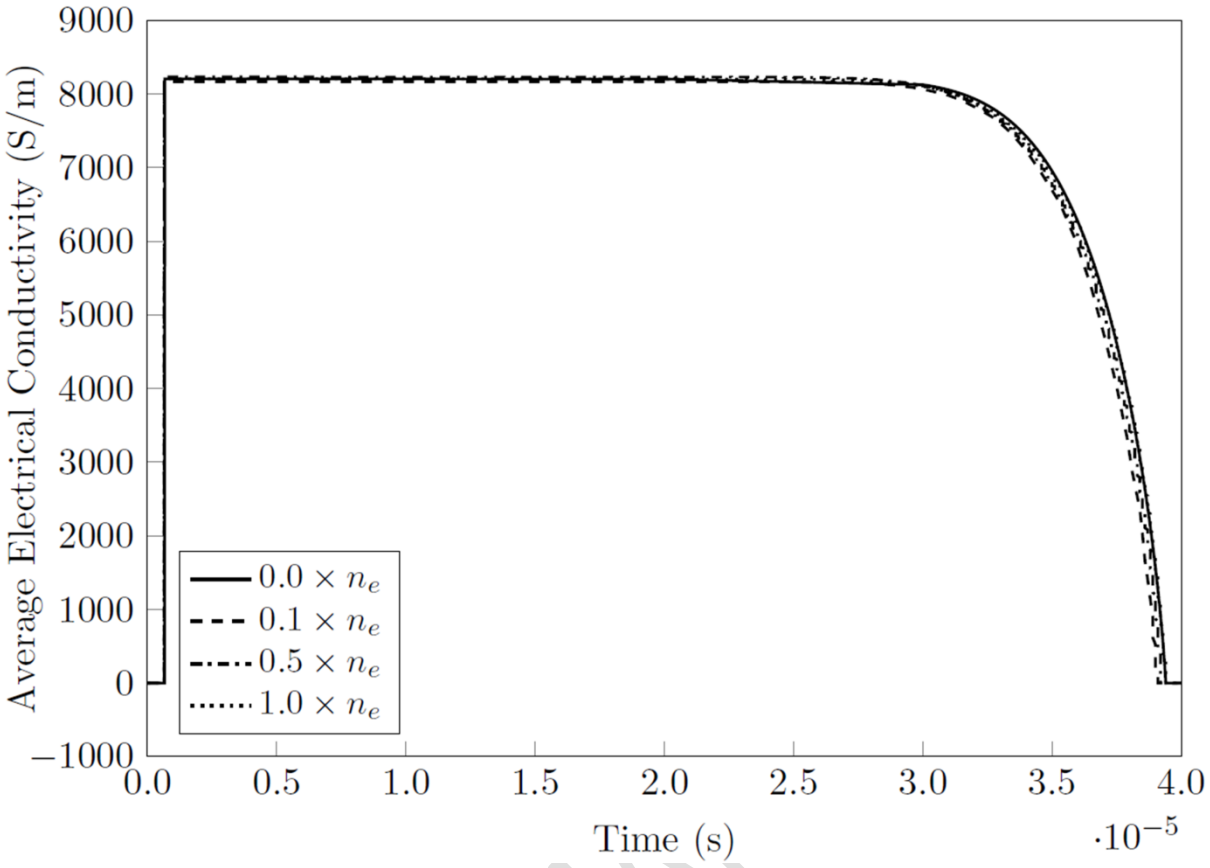

Figure 5 - Initial electrical conductivity of air for four test cases.

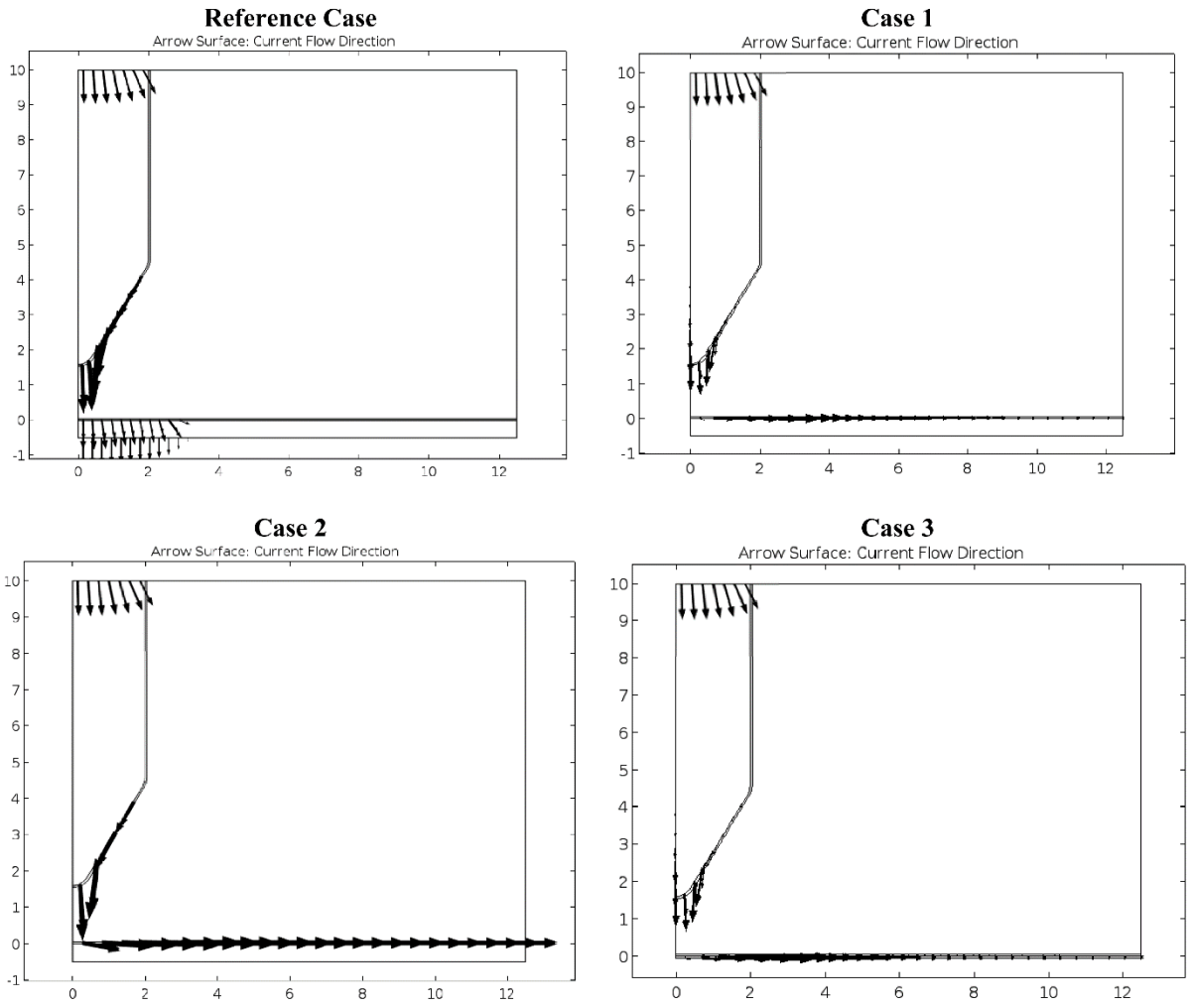

Figure 6 - Comparison of current flow paths for all cases.

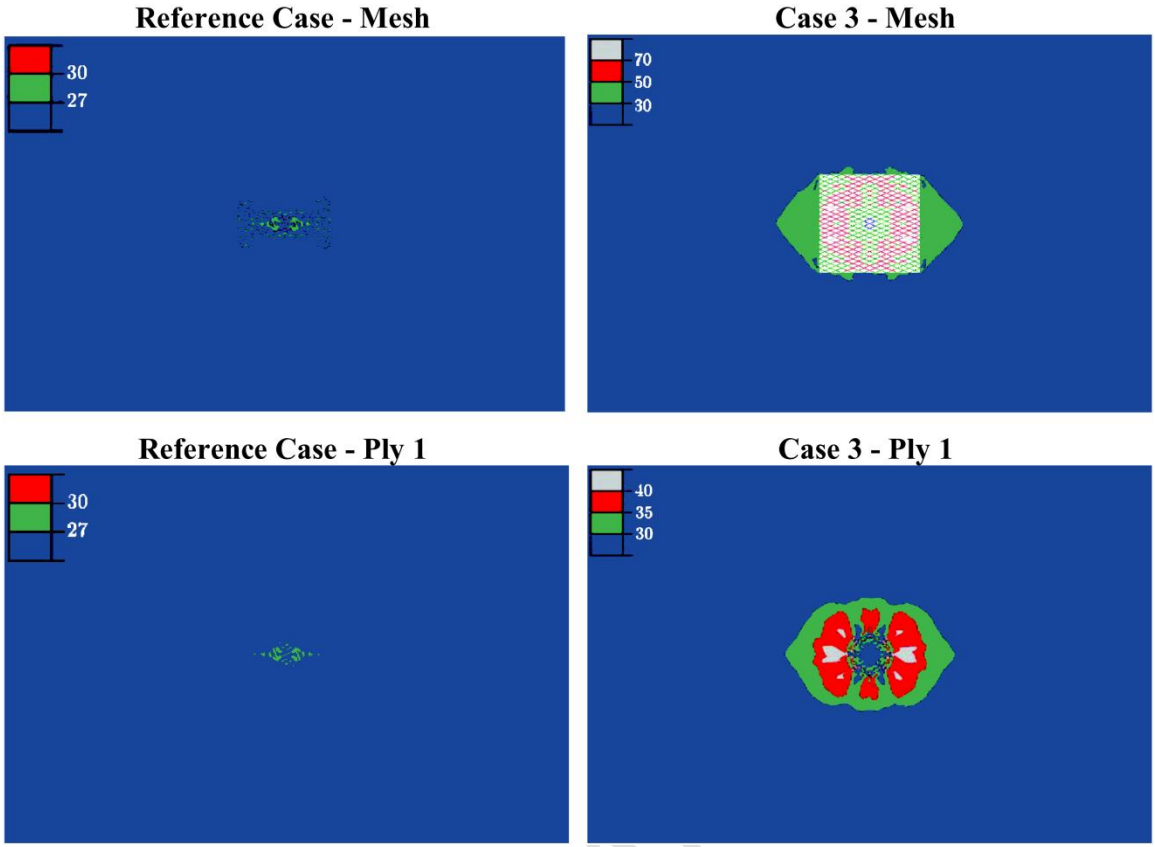

Figure 7 - Temperature contours for Reference and Case 3 thermal-electric simulations.

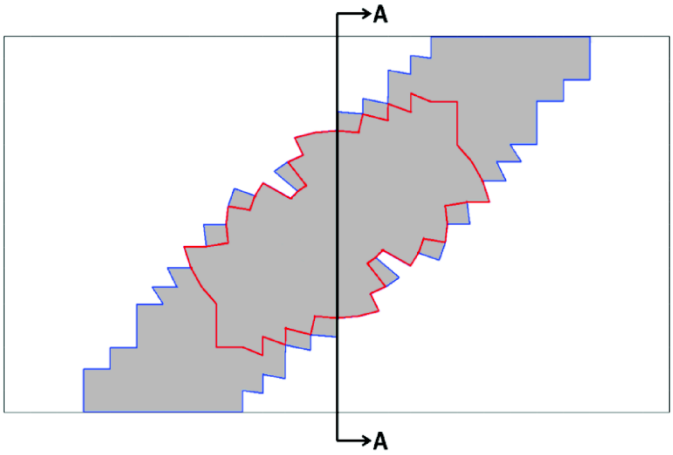

Top surface view of composite specimen. Grey zone represents damaged elements in moderate (blue) and severe zones (red), white zone represents pristine elements.

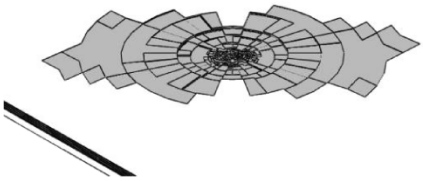

Isometric view of specimen top surface

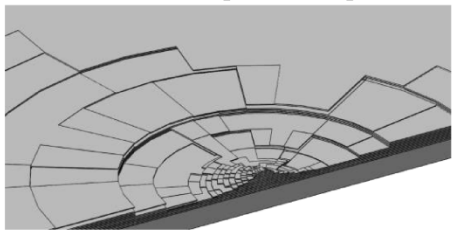

View of specimen Section A-A. Elements in severe damage zone removed for sub-surface damage visualisation.

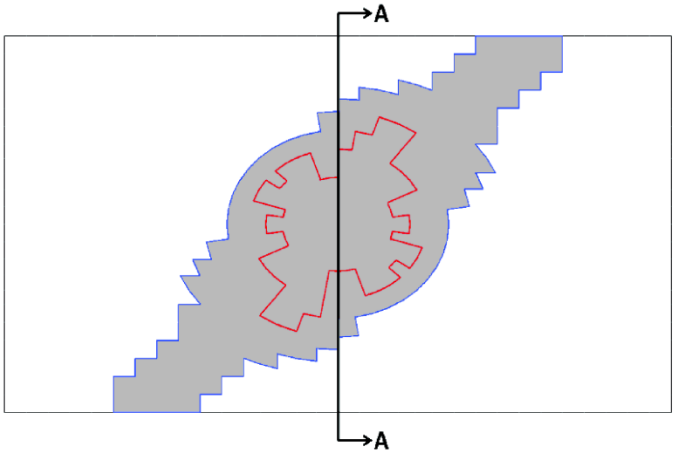

Top surface view of epoxy specimen. Grey zone represents damaged elements in moderate (blue) and severe zones (red), white zone represents pristine elements.

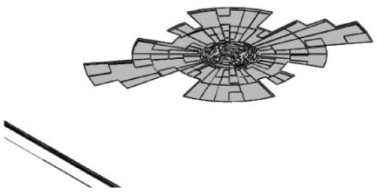

Isometric view of specimen top surface

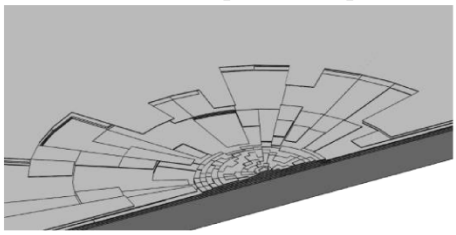

View of specimen Section A-A. Elements in severe damage zone removed for sub-surface damage visualisation.

Figure 8 - Case 1 and 2 severe damage volume representation (elements ≥500°C hidden)

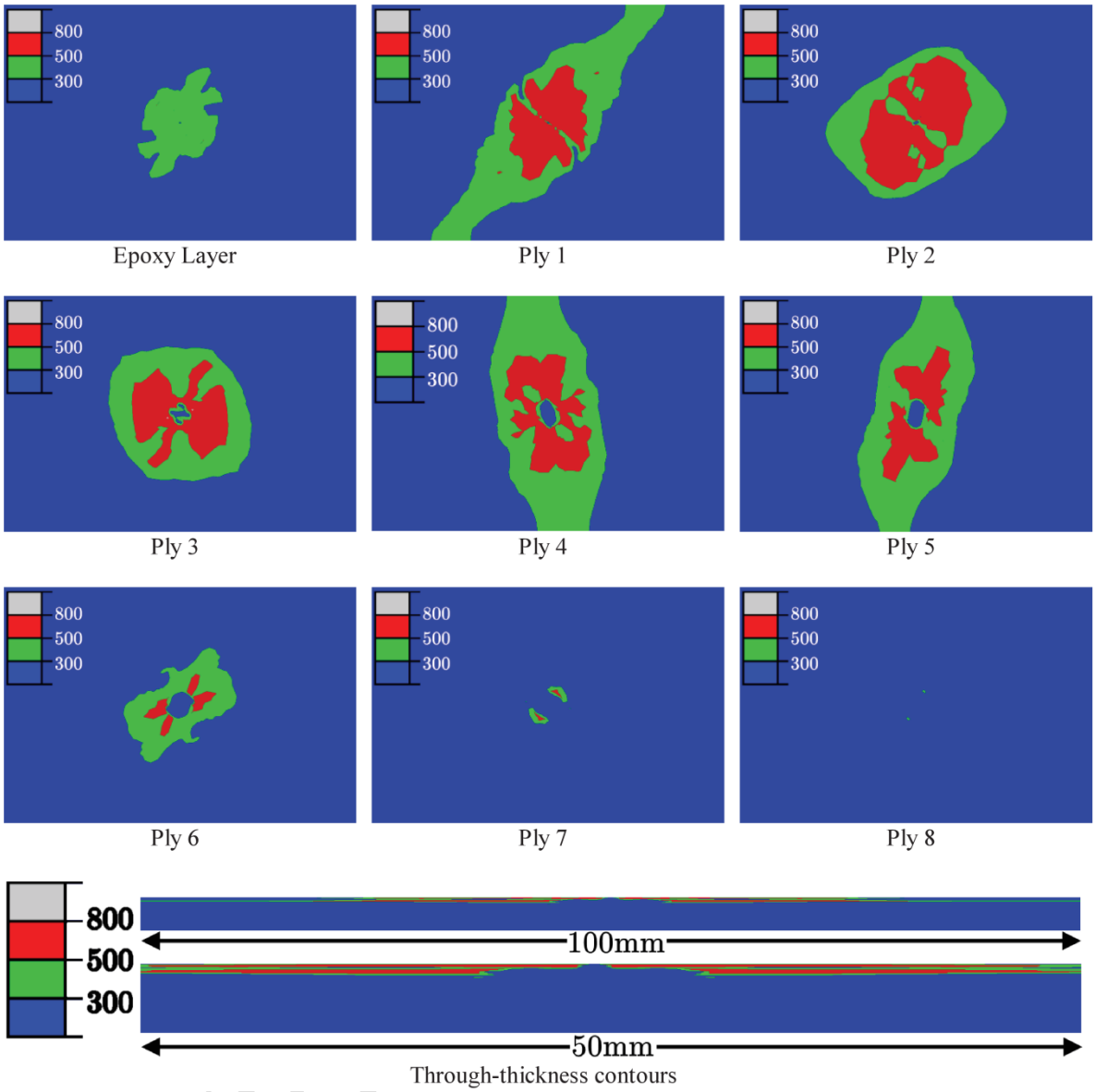

Figure 9 - Temperature contours for Case 1 thermal-electric simulation.

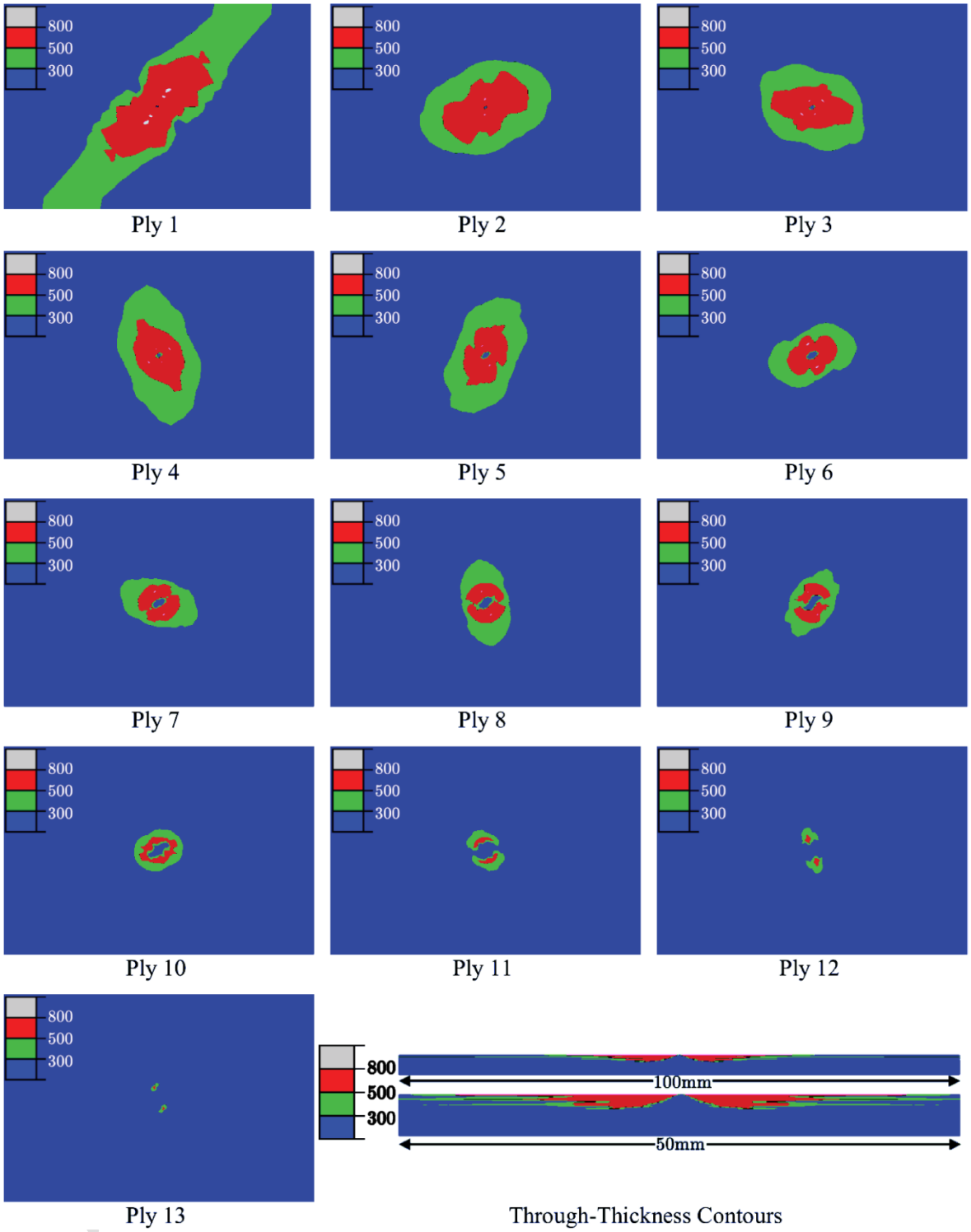

Figure 10 - Temperature contours for Case 2 thermal-electric simulation.